Desalination and Water Treatment
www.deswater.com
doi: 10.5004/dwt.2018.22315

114 (2018) 285–296
May

Efficient photocatalytic decolorization of methylene blue and victoria blue using reusable TiO_2 magnetic nanocomposite modified with zinc under UV irradiation: optimization via response surface methodology (RSM)

Marzieh Sadeghi*, Mohsen Irandoust, Hosna Azadi

Department of Chemistry, Razi University, Kermanshah, Iran, Tel./Fax: +98 8334274559; emails: negarsade@gmail.com, m.sadeghi@razi.ac.ir (M. Sadeghi), irandoust1341@yahoo.com (M. Irandoust), azadihosna@yahoo.com (H. Azadi)

Received 15 July 2017; Accepted 30 March 2018

ABSTRACT

In this work, photocatalytic decolorization of two commercial dyes, methylene blue (MB) and victoria blue B (VBB), under UV light irradiation using magnetic recyclable photocatalyst TiO_2, Fe_3O_4/TiO_2–SiO_2 modified with zinc in a self-made photoreactor, has been investigated. The prepared TiO_2 magnetic nanocomposite (TMN) can be well dispersed in the water and can be easily magnetic separated from the medium after adsorption. Scanning electron microscope, Fourier-transform infrared spectroscopy, X-ray diffraction, Brunauer–Emmett–Teller, and zeta potential sizer (Ξ) analyses were used to determine the sorbent characterization. Response surface methodology was employed to assess individual and possible interactions between the most effective parameters on the decolorization efficiency. Central composite design was applied for the optimization of photo-oxidative decolorization process. Predicted values of decolorization efficiency were found to be in good conformity with experimental values (R^2 = 98.8% and 99.5% and adjusted R^2 = 98.0% and 99.1% for MB and VBB, respectively). Optimization results showed that maximum decolorization efficiency was achieved at the optimum conditions catalyst dosage = 1.6 g L^{-1}, pH = 9, and irradiation time = 50 min for MB, and catalyst dosage =1.2 g L^{-1}, pH = 7.5, and irradiation time = 105 min for VBB. A comparison of the photocatalytic activity of nanocomposite TMN for the decolorization of MB and VBB under visible and UV light irradiation has been performed. Results showed that under UV light irradiation, photocatalytic activity increases, which may be due to high energy of photons. The photocatalyst TMN has significantly been reused for several times while their photocatalytic properties remained with trivial or no obvious change. This result demonstrates the high photocatalytic stability of the magnetic recyclable photocatalyst, Fe_3O_4/TiO_2–SiO_2 modified with zinc.

Keywords: Fe_3O_4/TiO_2–SiO_2 modified with zinc; Magnetic separation; Photocatalytic; Semiconductor; UV irradiation

1. Introduction

In the textile industry, dyeing process produced large volume of wastewater containing most unreacted colored dyestuffs. The presence of even a small amount of dye in water is highly visible and affects the water transparency and the gas solubility of water bodies [1]. From an environmental viewpoint, the disposal of synthetic dyes is of great concern, since dye effluents are aesthetic pollutants and can be toxic to organisms and human. Methylene blue (MB) and victoria blue B (VBB) are two kinds of cationic dyes, which are used widely in the industries [2]. Different removal technologies such as adsorption [2], biodegradation [3], chemical methods (e.g., chlorination and ozonation [4]), electrocoagulation, electrochemical reduction and oxidation, indirect electro-oxidation with strong oxidants, and photocatalytic degradation [5–10] have been recently developed. Over the last decade, advanced oxidation processes (AOPs) have attracted increasing interest as promising powerful methods for efficiently

* Corresponding author.

removing persistent organic pollutants from water [11,12]. In the AOPs, sufficient quantities of highly reactive and nonselective hydroxyl radicals can be produced that have the ability to oxidize most of the toxic and hazardous organic species present in industrial effluents [8].

Recently, heterogeneous photocatalyst is recognized as a new emerging AOP for the destruction of organic compounds present in the wastewater [13–18]. TiO_2 has confirmed to be the most suitable photocatalyst due to its low cost, nontoxicity, and photochemical stability. However, the industrial treatment of wastewater containing various organic pollutants using TiO_2–photocatalyst is uncommon because of the low efficiency of photodegradation. On the other hand, recombination of the produced electron-hole in the pure TiO_2 has limited its application in the photodegradation experiments [19]. For this reason, a great attention has been dedicated to improving the photocatalytic efficiency of TiO_2 [15–19]. The design of composite oxides mixed by titania has been reported as a promising way to achieve high photocatalytic activity [16–18]. It has been found that ZnO improves photocatalytic activities of TiO_2 [20]. Besides, compared with TiO_2, ZnO has the ability to absorb a large fraction of the UV light [20–24]. Therefore, it is expected that the composite of TiO_2/ZnO exhibits more efficient in photocatalytic degradation. However, the difficulty in separating and recovering nanosized powders from the treated solution, due to the formation of milky dispersions after mixing the powder catalyst in water, seriously limits their practical applications. TiO_2 magnetic nanocomposites (TMNs) can overcome this drawback. Several works have been performed on the use of magnetic nanocomposites to remove toxic dye from wastewater [16–18,21]. The magnetic separation provides a suitable route for and efficient removal of the catalysts from a large volume of wastewater. It is assumed to avoid the agglomeration and loss of catalysts, and thus, it increases catalytic reusability [21]. Several examples of applications employing iron oxide with titania have been reported [17,18]. However, it is obvious that both γ-Fe_2O_3 and Fe_3O_4 face the risk of conversion since either of these compounds may be unstable crystal structure iron oxide. The aforementioned problem can be addressed by the introduction of the coating on the surface of iron oxide nanoparticles.

In this research, the new synthesized TMN, Fe_3O_4/TiO_2–SiO_2, modified with zinc for photocatalytic decolorization of MB and VBB was prepared via sol–gel method. The single dimensional search is laborious, time consuming, and incapable of reaching the true optimum due to ignoring the interaction among variables. To resolve this problem, response surface methodology (RSM) has been proposed to study of simultaneous effects of experimental variable and optimize them. RSM can analyze interactions of influencing experimental factors and determine the optimum region of the factors level at minimum number of designed experiments [22,23]. Variables affecting the performance of photocatalytic decolorization were thoroughly investigated. A central composite chemometrics design was applied for multivariate optimization of the effects of three different parameters influencing the photocatalytic decolorization efficiency of the dye solution containing MB and VBB using UV/TMN nanocomposite process. RSM was used to investigate the individual effects and possible interactions between the most effective variables, including the reaction time, catalyst dosage, and pH solution. A comparison the photocatalytic activity of TiO_2 nanocomposite for the decolorization of MB and VBB under UV and visible light irradiation has been investigated. Results demonstrated the enhancement of photocatalytic activity under UV light irradiation rather than visible light. The photocatalytic stability of the TiO_2 nanocomposite has also been checked. After six successive cycles, these TMNs were magnetically separated from the treated solution.

2. Experimental methods

2.1. Reagents

All the reagents were of analytical grade and used as received without further purification. All chemicals including NaOH, HCl, $Fe(NO_3)_3.9H_2O$, tetraethyl orthosilicate, titanium isopropoxide, ethanol, oxalic acid, and $Zn(NO_3)_2.6H_2O$ with the highest purity available are purchased from Merck, Dermasdat, Germany. MB was purchased from Merck, and VBB was obtained from Sigma–Aldrich. The double distilled water was used to prepare experimental solutions.

2.2. Instruments

Spectrophotometric analyses were carried out with an Agilent UV–visible spectrophotometer model 8453 with diode array detector at a wavelength of 663 and 590 nm for MB and VBB, respectively. The chemical structure of TiO_2 nanocomposite was directly analyzed by a (BRUKER-German) FTIR spectrophotometer using KBr pellets. Surface morphology of the nanocomposite was observed using a (Hitachi S-4800) scanning electron microscope (SEM). Brunauer–Emmett–Teller (BET) analysis for specific surface area and pore volume was measured using a (NOVA 2200 instrument, Quantachrome, USA). X-ray diffraction (XRD) pattern was collected with an automated Philips X 'Pert (40 kV and 30 mA) X-ray diffractometer with Cu Kα radiation source (λ = 1.542 Å). The magnetic measurements were performed using a vibrating sample magnetometer (VSM; BHV-55, Riken, Japan) at room temperature. The shaker and incubator (DK-S1060, Korea) were used to conduct all the experiments. The pH of solutions was adjusted with very small amounts of 0.01 M hydrochloric acid and sodium hydroxide and determined using Jenway 3345 pH meter.

2.3. Synthesis of TiO_2 magnetic nanocomposite

The modified Fe_3O_4/TiO_2–SiO_2 used in present study was prepared as reported in our previous work by a combination of sol–gel and wetness impregnation methods [24,25]. Fe_3O_4/TiO_2–SiO_2 modified with zinc was synthesized in two steps. At first 1.0 mL of titanium isopropoxide, 1.4 g of $Fe(NO_3)_3.9H_2O$ and 0.25 mL of tetraethyl orthosilicate were dissolved in 100 mL ethanol; the mixture were stirred for 10 min at 45°C. After that, 0.15 g of oxalic acid was added to the mixture under rigorous stirring at same temperature. After 90 min, the homogeneous solutions were obtained almost. The solutions have been left at room temperature and air atmosphere to gellify. The obtained gel was dried in the oven at 100°C for 10 h to give a material denoted as the precursor. After drying and

milling of precursor, it was thermally treated (calcination) at 450°C for 6 h to give the Fe_3O_4/TiO_2–SiO_2. In next steps, 1.0 g of calcined precursor was impregnated with aqueous solution of $Zn(NO_3)_2.6H_2O$ (10 mL, 0.02 mol L^{-1}). At this step, new precursor has been dried at 100°C for 10 h and calcined at 450°C for 6 h again. The final powder is Fe_3O_4/TiO_2–SiO_2 that was modified with zinc.

2.4. Experimental system and photocatalytic activity measurement

The self-made photocatalytic system used in this study was illustrated in Fig. 1 that consists of three parts: a sealed box with aluminum foil to shield it from external light sources, a Pyrex reactor cell with a 12 cm height and an effective volume of 250 mL, and a medium pressure mercury UV lamp type Philips (75W, λ_{max} = 365 nm), which was positioned on top of the reactor cell as shown in Fig. 1. Visible light irradiation was carried out using 150 W halogen lamp. The distance from the lamp to the top of the reactor was 12 cm. An air pump provides compressed air to ensure a constant supply of oxygen in air to the reaction volume and complete mixing of solution and photocatalyst during the photoreaction. During the reaction, a water-cooling system cooled the water jacketed photochemical reactor to maintain the solution at 25°C ± 1°C.

The photocatalytic activity of the TMN nanocomposite system under UV irradiation was evaluated using MB and VBB as the target compounds. The photocatalytic experiment was performed at room temperature under a UV tube light. The proper amount of the photocatalyst (1.6 and 1.2 g L^{-1} for MB and VBB, respectively) was suspended in 250 mL of standard dye aqueous solution with the concentration of 30.0 mg L^{-1} for MB and (50.0 mg L^{-1}) for VBB. The distance between solution and UV source was constant, 12 cm, in all experiments. Prior to the UV light illumination, the suspension was shacked for 20 min to allow adsorption–desorption equilibrium on the TMN nanocomposite surface. At different reaction times obtained with experimental design, 2.0 mL sample was taken, and the equilibrium concentrations of dyes were measured after magnetic separation using the permanent magnet, with a UV–Vis spectrophotometer at λ_{max} 663 and 590 nm for MB and VBB, respectively. The removal percentage of dye was calculated using the following equation (Eq. (1)):

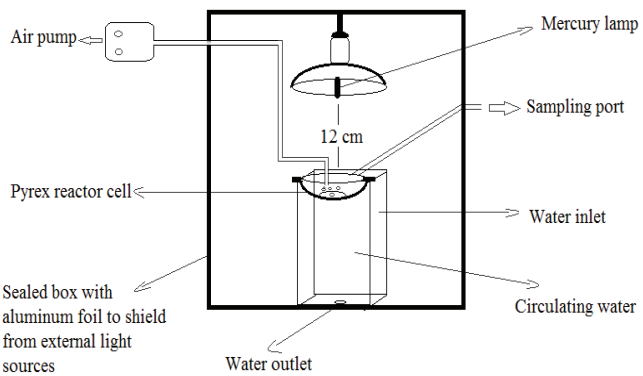

Fig. 1. Schematic diagram of the self-made photocatalytic setup.

$$\text{Removal (\%)} = (C_0 - C_t)/C_0 \times 100 \quad (1)$$

where C_0 (mg/L) and C_t (mg/L) are the dye concentration at initial and after time t, respectively.

The aerating rates of air and reacting temperature were adjusted at 30 mL min^{-1} and 25°C, respectively.

2.5. Experimental design (response surface methodology) studies

In the present study, central composite design (CCD), which is a widely used form of RSM, was employed for the optimization of photocatalytic decolorization process. In order to evaluate the influence of operating parameters on the photocatalytic decolorization efficiency of MB and VBB, three main factors were chosen: catalyst dosage (X_1), pH (X_2), and irradiation time (X_3). The photodegradation percent (% removal) of dyes (MB and VBB) was considered as response variable (Y). A total of 36 experiments were employed in this work, 18 experiments for the MB, and 18 experiments for VBB. The obtain regression equations were further applied to systematic investigation of the main and interactive effects of the independent variables on the responses. In this study, for three variables (n = 3), the design includes 2^n (2^3 = 8) cubic points, $2n$ (2 × 3 = 6) axial or star points, and 4 replicates of the center point in order to estimate the experimental error. The cubic points implicate a full two-level factorial design with coded values of –1 and +1 (–1 and +1 indicate lower and upper levels of each variable, respectively). In CCD, the axial points define the points in which two variables are in their central level (coded as 0) and other variable situated at a defined distance from the center of the design (–α and +α). It should be noted that for a face-central CCD, $|\alpha|$ = 1, and therefore, each variable was studied at three different levels (–1, 0, +1). Experimental data were analyzed using Design-Expert software (Trial Version 8.0.0, Stat-Ease Inc., Minneapolis, MN, USA) for coded value of the variables. The experimental ranges and the levels of the independent variables for MB and VBB removal are given in Table 1. It should be noted that the extreme values for each variable were selected after running a series of preliminary ones at the time experiments.

3. Results and discussion

3.1. Characterization of TiO_2 magnetic nanocomposite

The XRD pattern of the Fe_3O_4/TiO_2–SiO_2 that modified by zinc [Fe/(TiO_2–SiO_2) = 40 wt% and Zn/(TiO_2–SiO_2) = 4 wt%] is depicted in Fig. 2. The recognized phases were TiO_2 (tetragonal), Fe_2O_4Zn (cubic), and SiO_2 (amorphous). From the XRD data, according to Debye–Scherrer equation [26], the crystallite size was 56 nm.

The morphology samples were investigated by SEM of TMN nanoparticles (Fig. 3). As can be seen from Fig. 3, the morphology of the precursor and calcined sample are clearly different. Several larger agglomerations of particles were seen in precursor; meanwhile, after calcination of precursor at 450°C for 6 h, more homogeneous morphology with reduction of agglomerate size can be seen from Fig. 3(b). It may be due to the coating of calcined sample surface by small crystallites of iron oxides and zinc oxide. It can be estimated that the average particle size of Fe_3O_4/TiO_2–SiO_2 that was

Table 1
Experimental ranges and levels of the independent test variables for MB and VBB

Coded factor	Factor	MB level			VBB level		
		–1	0	1	–1	0	1
X_1	Catalyst dosage (g L^{-1})	0.1	0.9	1.7	0.2	0.7	1.2
X_2	pH	3	6	9	3	6	9
X_3	Irradiation time (min)	10	30	50	15	60	105

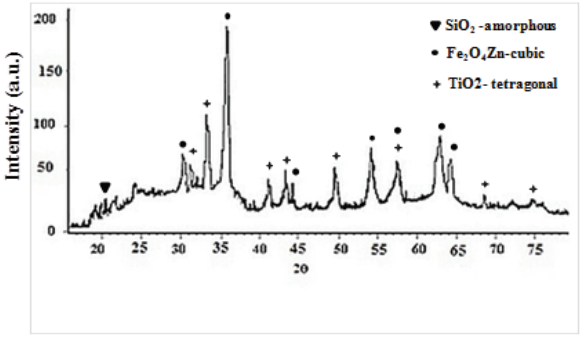

Fig. 2. XRD pattern of Fe_3O_4/TiO_2–SiO_2 sample modified by zinc.

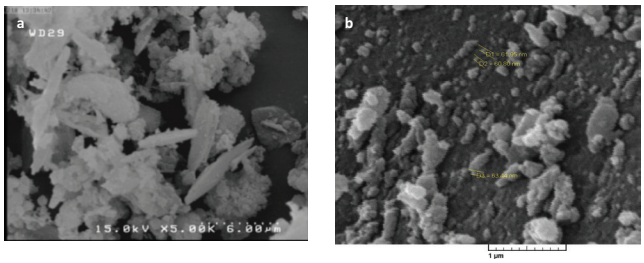

Fig. 3. The SEM images of Fe_3O_4/TiO_2–SiO_2 sample modified by Zn: (a) precursor and (b) calcined sample.

modified by zinc (TMN) is 61 nm, which is in agreement with the XRD data (56 nm).

The result of VSM measurements was displayed on the hysteresis curve of Fe_3O_4/TiO_2–SiO_2 that is modified by zinc (Fig. 4). The shape of that hysteresis curve resembles a superparamagnetic behavior [27]. Magnetic saturation values were produced by Fe_3O_4/TiO_2–SiO_2 that was modified by zinc at applied field of 8,500 (Oe) is 10.0 emu/g. The magnetic TMN exhibits a superparamagnetic state with small residual magnetization at room temperature, which is desirable for many useful applications,

The Fourier-transform infrared spectroscopy (FTIR) spectra of the precursor and calcined sample were measured to confirm the composition and structure of the nanocomposites (Fig. 5). It has been reported that the band at the wave number about 910–960 cm^{-1} corresponds to Si–O–Ti vibration; 500–900 cm^{-1} originates from Ti–O–Ti [28,29]. As can be seen from Fig. 5, the peaks at 1,068 and 484 cm^{-1} were due to asymmetric stretching and bending modes of Si–O–Si linkage in precursor and those at 461and 1,074 cm^{-1}

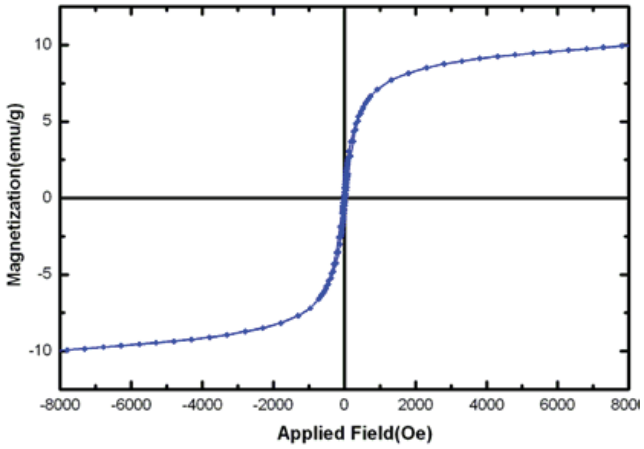

Fig. 4. Magnetization curve for Fe_3O_4/TiO_2–SiO_2 sample modified by Zn.

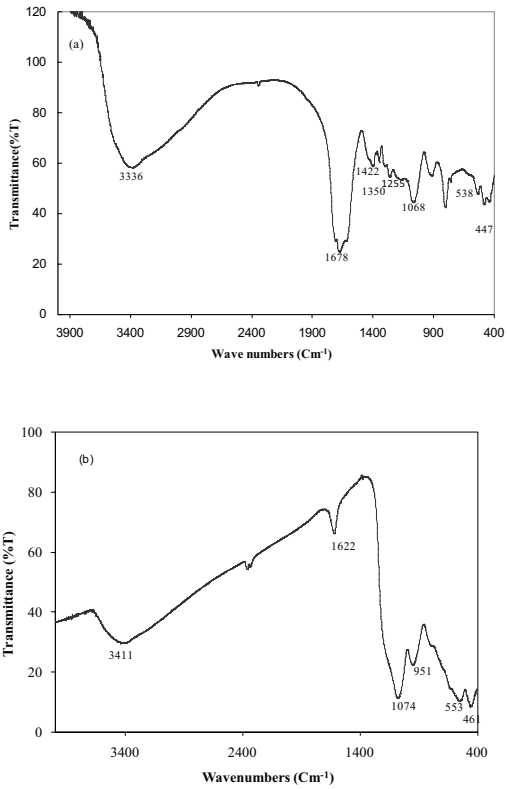

Fig. 5. FTIR spectra of the Fe_3O_4/TiO_2–SiO_2 promoted with Zinc: (a) precursor and (b) calcined sample.

were corresponded to the calcined sample [30]. The peak about 2,300 cm^{-1} was due to Fe–O–Ti in both of precursor and calcined TMN [31]. The bands at 538 and 553 cm^{-1} were attributed to the Fe–O stretching in Fe–O–Si bonds [32] in precursor and calcined catalyst, respectively. These results showed that the Fe–SiO_2 interaction exists in the catalyst in a form of Fe–O–Si structure [33]. By combining the results of FTIR and XRD, one can see that silica exists as a segregated amorphous phase in the anatase titania.

The specific surface area and porosity of the $Fe_3O_4/SiO_2/TiO_2$ promoted with zinc composite structures were investigated by N_2 adsorption–desorption isotherm. The specific surface area for calcined TMN is 187.2, 188.4, and 189.2 $m^2 g^{-1}$ using BET, BJH, and DH methods, respectively. Pore diameter and pore volume were estimated to 0.7426 A and 15.93 $cm^3 g^{-1}$, respectively.

3.2. Photocatalytic active of TiO_2 nanocomposite under visible and UV light irradiation

To elucidate the photocatalytic efficiency under different light irradiation, a set of experiments were done by changing light irradiation as visible and UV. In order to study the effect of light on photocatalytic activity, the experiment was also done under dark condition. Fig. 6 shows the comparison of color removal efficiency of MB and VBB with various light sources. The higher photocatalytic efficiency was achieved under UV light irradiation than visible light. It can be attributed to the high energy of photons. Besides the band gap of ZnO used is 3.19 eV, it absorbs UV light effectively. Under dark condition, 31% and 40.3% of the MB and VB, respectively, dye molecules have been adsorbed in 20 min; then, desorption was occurred slowly and reached 17.6% in 60 min for MB and 19.7% in 120 min for VB. According to the result under dark conditions, the photocatalyst can be employed as a good adsorbent for the removal of organic contaminants. Despite the fact that the UV irradiation can achieve preferable results in the decolorization of dyes than that of visible light, visible light will turn up as an alternative light source due to its accessibility and nonhazardous nature.

The photocatalytic mechanism is believed to proceed as follows:

$$TMN + hv \rightarrow e^-_{CB} + h^+_{VB} \quad (2)$$

$$h^+_{VB} + H_2O \rightarrow OH^\bullet + H^+ \quad (3)$$

$$e^-_{CB} + O_2 \rightarrow O_2^\bullet \quad (4)$$

$$2O_2^{\bullet\circ} + H_2O \rightarrow HO_2^\bullet + {}^\bullet OH \quad (5)$$

$${}^\bullet OH + {}^\bullet OH \rightarrow H_2O_2 \quad (6)$$

$$O_2^{\bullet\circ}/OH^\bullet + \text{dye} \rightarrow \text{Mineralized product} \quad (7)$$

When the photocatalyst is exposed to light, the holes (h^+) and electrons (e) are produced in the valence band and conduction band of the photocatalyst simultaneously (Eq. (2)) [34]. Then, the h^+ will react with the hydroxyl groups or water molecules to produce hydroxyl radicals (Eq. (3)). The conduction e can be scavenged by the dissolved O_2 on the surface of the catalyst to form superoxide radical anions (O_2°) and further generate HO_2° (Eqs. (4) and (5)). Hydrogen peroxide (H_2O_2) will be formed by the reaction between one HO° and another (Eq. (6)). Finally, a dye molecule could be largely oxidized by the photogenerated O_2°, $^\circ OH$, and H_2O_2 radicals and generates a mineralized product like CO_2, H_2O, etc. (Eq. (7)).

Fig. 7 shows the decolorization of MB and VBB dyes under irradiation in the time interval of 50 min and 120 min and in the presence of TMN catalyst. The decrease of absorption spectra demonstrates decolorization of the dyes in the applied conditions. There are no additional peaks appearing in the UV–Vis spectra, which show the dyes are completely degraded. Formation of (2-amino-5-*N*,*N*-dimethylphenyl)

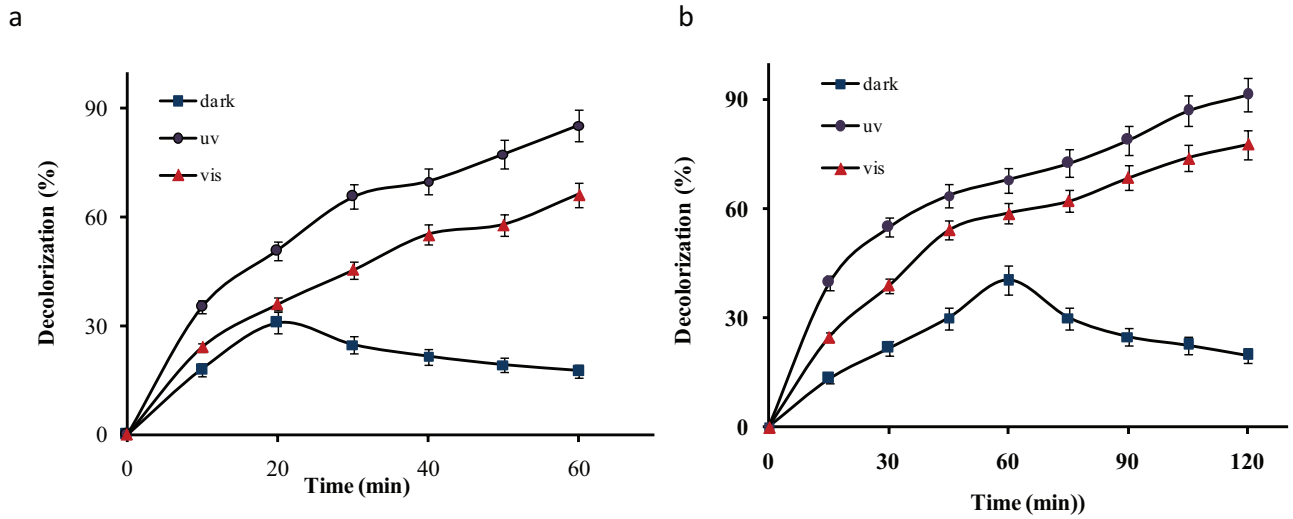

Fig. 6. Comparisons of color removal efficiency of (a) MB, conditions: TMN = 1.0 g L^{-1}, MB = 30 ppm, pH = 9.0, λ_{max} = 663 nm and (b) VB, conditions: TMN = 1.0 g L^{-1}, VBB = 60 ppm, pH = 7.5, λ_{max} = 590 nm, with various light sources.

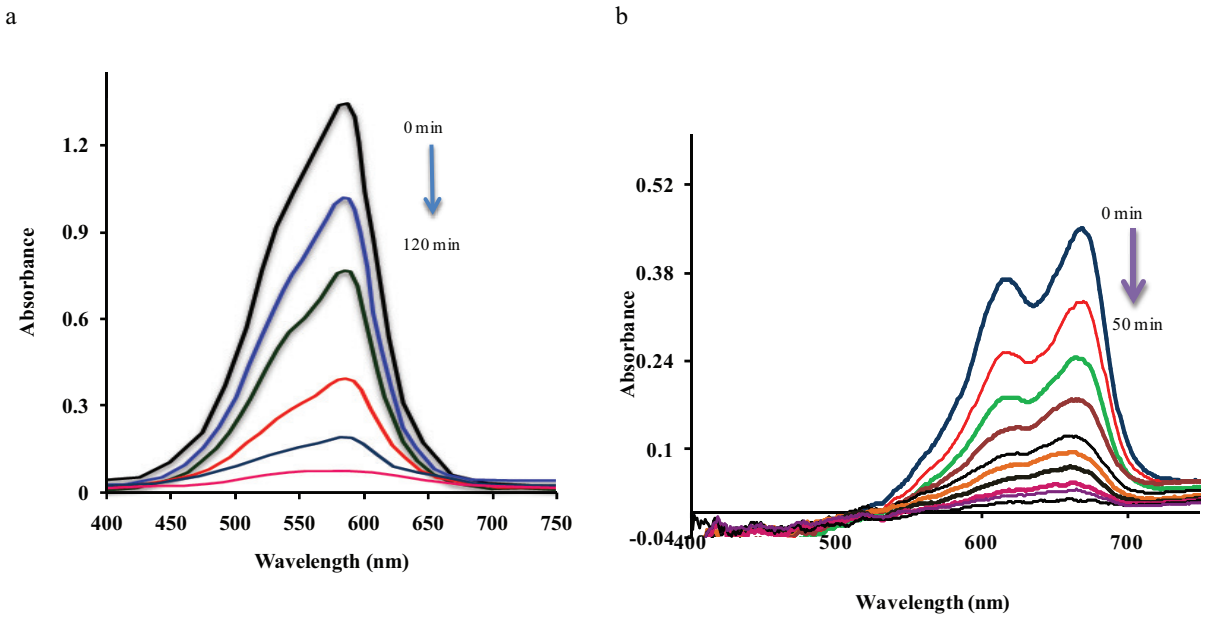

Fig. 7. Decrease absorption spectra of: (a) Victoria blue B (45 ppm, 0–120 min) and (b) MB (20 ppm, 0–50 min) in the presence of TMN photocatalyst (1.0 g L^{-1}).

3-*N*,*N*-dimethylphenylsulfoxide (*m*/*z* = 303), 4-amino-2-sulfo-*N*-methylformanilide (*m*/*z* = 230), 4-*N*,*N*-dimethylaniline (*m*/*z* = 136), 3,4-dihydroxy-*N*-methylformanilide (*m*/*z* = 167), and 3,4-dihydroxyaniline (*m*/*z* = 125) were observed as the degradation products in GC–MS analysis of the photodegraded solution of MB [35]. The degradation mechanisms for MB were reported in the literature [34–36].

3.3. Central composite design model

CCD included the following steps: at first, statistically designed experiments were done, and then, factors and levels were selected; after that, the coefficients of the mathematical model were estimated in order to predict the response and check its adequacy. The 3-factor CCD matrix for 18 experimental sets and observed results of photocatalytic decolorization (removal %) for MB and VBB are shown in Tables 2 and 3, respectively. The second-order polynomial response equation (Eq. (8)) was used to correlate the dependent and independent variables.

$$y = \beta_0 + \beta_1 x_1 + \beta_2 x_2 + \beta_{11} x_1^2 + \beta_{22} x_2^2 + \beta_{12} x_1 x_2 + \text{Residual} \quad (8)$$

where y is a response variable of photocatalytic decolorization percent (removal %); b_i is regression coefficients for linear effects; b_{ik}, the regression coefficients for quadratic effects, and x_i coded experimental levels of the variables. Based on these results, an empirical relationship between the photocatalytic decolorization and independent variables was achieved and expressed by the following second-order polynomial equations. Based on the experimental results, photocatalytic decolorization (removal %) of dyes have been predicted by second-order polynomial equations (Eqs. (9) and (10)), respectively, and presented in Tables 2 and 3. These results indicated good agreements between the experimental and predicted values of photocatalytic decolorization.

$$y = 66.45 + 10.42X_1 + 5.42X_2 + 25.57X_3 + 3.73X_2X_3 - 6.74X_1^2 + 3.86X_2^2 - 10.6X_3^2 \quad (9)$$

$$y = 68.99 + 25.25\,X_1 + 21.75\,X_2 + 18.69\,X_3 + 3.91\,X_1X_2 - 6.05\,X_1^2 - 12.05\,X_2^2 - 8.51\,X_1^2X_2 - 13.11\,X_1X_2^2 \quad (10)$$

The regression coefficients for each term of the full quadratic models and their analysis of variance (ANOVA) at a 95% confidence level for MB and VBB were shown in Tables 4 and 5, respectively. ANOVA is needed to examine the significance and suitability of the model. As can be seen in Tables 4 and 5, the F values for MB and VBB models (120.26 and 245.35) were obviously greater than the tabulated F (F_C) confirming the adequacy of the models fitted. On the other hand, corresponding p-value ($p < 0.0001$) confirms that only a 0.01% of the model results could arise from noise.

The lack-of-fit (LOF) term shows the variation in the data around the fitted model and when it is significant confirms that the fitted model cannot fit the data well [37]. Here, the LOF p-values (VBB: 0.0531 > 0.05 and $F_{cal} = 8.55 < F_C = 8.94$; MB: 0.2101 > 0.05, and $F_{cal} = 2.85 < F_C = 8.87$) implied the variation of the data around the fitted models were not significant relative to the pure error.

The R-square test (R^2) has been also used for the validation of the mathematical model. Experimental results and the predicted values calculated by the models (Eqs. (9) and (10)) are reported in Tables 4 and 5. The predicted values match the experimental values reasonably well with R^2 of 0.988 and 0.9954 for MB and VBB, respectively.

According to the ANOVA results, the model R^2 value, which equals 0.988 and 0.9954 for MB and VBB, respectively, ensures a satisfactory adjustment of the model to the

Table 2
CCD matrix for three variables (actual and coded levels) with the observed and predicted values of removal percentage of MB

Run	Variable X_1; dose (g L^{-1})	Variable X_2; pH	Variable X_3; time (min)	Removal (%)	
				Observed	Predicted
1	1.7 (+1)	9 (+1)	50 (+1)	98.9	98.1
2	0.1 (–1)	9 (+1)	50 (+1)	79.8	77.3
3	1.7 (+1)	3 (–1)	50 (+1)	83.1	79.8
4	0.1 (–1)	3 (–1)	50 (+1)	55.3	59.0
5	1.7 (+1)	9 (+1)	10 (–1)	40.2	39.5
6	0.1 (–1)	9 (+1)	10 (–1)	19.7	18.7
7	1.7 (+1)	3 (–1)	10 (–1)	34.1	36.1
8	0.1 (–1)	3 (–1)	10 (–1)	15.3	15.3
9	0.9 (0)	6 (0)	50 (+1)	78.5	81.4
10	0.9 (0)	6 (0)	10 (–1)	30.6	30.3
11	0.9 (0)	9 (+1)	30 (0)	70.7	75.7
12	0.9 (0)	3 (–1)	30 (0)	67.3	64.9
13	1.7 (+1)	6 (0)	30 (0)	67.4	70.1
14	0.1 (–1)	6 (0)	30 (0)	49.4	49.3
15	0.9 (0)	6 (0)	30 (0)	68.2	66.4
16	0.9 (0)	6 (0)	30 (0)	64.8	66.4
17	0.9 (0)	6 (0)	30 (0)	69.8	66.4
18	0.9 (0)	6 (0)	30 (0)	68.3	66.4

Table 3
CCD matrix for three variables (actual and coded levels) with the observed and predicted values of removal percentage of VBB

Run	Variable X_1; dose (g L^{-1})	Variable X_2; pH	Variable X_3; time (min)	Removal (%)	
				Observed	Predicted
1	1.2 (+1)	9 (+1)	105 (+1)	99.2	98.3
2	0.2 (–1)	9 (+1)	105 (+1)	67	66.2
3	1.2 (+1)	3 (–1)	105 (+1)	64.8	65.3
4	0.2 (–1)	3 (–1)	105 (+1)	45.6	45.1
5	1.2 (+1)	9 (+1)	15 (–1)	60	60.7
6	0.2 (–1)	9 (+1)	15 (–1)	28	29.4
7	1.2 (+1)	3 (–1)	15 (–1)	25.8	24.9
8	0.2 (–1)	3 (–1)	15 (–1)	12.1	13.2
9	0.7 (0)	6 (0)	105 (+1)	87	85.9
10	0.7 (0)	6 (0)	15 (–1)	50.8	51.8
11	0.7 (0)	9 (+1)	60 (0)	81	80.1
12	0.7 (0)	3 (–1)	60 (0)	37.5	36.6
13	1.2 (+1)	6 (0)	60 (0)	90.5	91.7
14	0.2 (–1)	6 (0)	60 (0)	40	38.7
15	0.7 (0)	6 (0)	60 (0)	68.7	69.3
16	0.7 (0)	6 (0)	60 (0)	68	67.2
17	0.7 (0)	6 (0)	60 (0)	68.4	67.6
18	0.7 (0)	6 (0)	60 (0)	67.9	68.3

experimental data and indicates the high predictive power of the models. This implies that 98.8% and 99.54% of the variations for MB and VBB, respectively, dyes removal efficiency are explained by the selected variables. Adjusted R^2 (Adj-R^2) is also a tool for measuring the goodness of a fit, but it is more convenient for comparing models with different numbers of independent factors. Here, adjusted R^2 values 0.980 and 0.9914 for MB and VBB, respectively, were very close to the corresponding R^2 values. Usually, it is important to confirm if the chosen model provides adequate approximation of the real system. The correlation between the observed and predicted values for MB and VBB are depicted in Fig. 8. The

Table 4
Analysis of variance (ANOVA) for the fit of decolorization efficiency from CCD for MB

Source	SS[a]	df[b]	MS	*F*-value	F_C	*p*-value
Model	8,819.27	7	1,259.896	120.2608	3.1355	<0.0001
Residual	104.7636	10	10.47636			
LOF	91.05673	7	13.0081	2.847061	8.8867	0.2101
Pure error	13.70688	3	4.568958			

[a]Sum of squares.
[b]Degrees of freedom.
Note: R^2: 0.988, adjusted R^2: 0.980, and predicted R^2: 0.955.

Table 5
Analysis of variance (ANOVA) for the fit of decolorization efficiency from CCD for VBB

Source	SS[a]	df[b]	MS	*F*-value	F_C	*p*-value
Model	9,581.31	8	1,197.66	245.35	3.2296	<0.0001
Residual	43.93	9	4.88			
LOF	41.51	6	6.92	8.55	8.9406	0.0531
Pure error	2.43	3	0.81			

[a]Sum of squares.
[b]Degrees of freedom.
Note: R^2: 0.9954, adjusted R^2: 0.9914, and predicted R^2: 0.9307.

points were located very close to the diagonal line indicating low discrepancies between them. The comprehensive description on *F* values and goodness of the model and interaction effect for photocatalytic degradation of pollutants is presented in literature [37,38].

In the case of MB, considering the confidence level of 95%, the regression coefficients with *p*-value lower than 0.05 are coefficients, which have a significant effect on the response. The *p*-values indicate that linear effects of all variables and quadratic term of X_1 (catalyst dosage) and X_3 (irradiation time) as well as binary interaction between X_2 and X_3 (pH and time) could be considered as significant model terms ($p < 0.05$; Table 6). In the case of VBB, the results of ANOVA for the reduced cubic model terms after applying stepwise strategy for eliminating nonsignificant terms are shown in Table 7. As can be seen, linear effects of all variables and quadratic term of X_1 (catalyst dosage) and X_2 (pH) as well as interaction between X_1 and X_2 could be considered as significant model terms ($p < 0.05$).

3.4. Effect of variables as response surface

As discussed in the previous section, an experimental design model (CCD) and RSM were used with three variables to evaluate their effect on the dye decolorization efficiency. The final models were expressed as three-dimension surface plots to visualize the relationship between the response and the experimental levels of each factor.

Figs. 9(a)–(c) (left) show the effect of time and pH, pH and catalyst dosage, and time and catalyst dosage on the MB decolorization efficiency, respectively, each one at the central level of the third variable. Figs. 9(a)–(c) (right) also shows the effect of pH and catalyst dosage, time and pH, and time and catalyst dosage on the on VBB decolorization efficiency removal, respectively, each one at the central level of the third variable.

In Figs. 9(a) (left) and 9(b) (right), the response surface plots MB and VBB were developed as a function of pH and reaction time while the catalyst dosage was kept constant at 0.9 and 0.7 g L^{-1} for MB and VBB, respectively, being the central levels. As can be seen in Fig. 9(a) (left), irradiation time had a significant effect on decolorization efficiency of MB; it increased with increasing reaction time at all applied pH, and also decolorization efficiency increased with increasing pH. As can be seen in Fig. 9(b) (left), decolorization efficiency increased with increasing pH and irradiation time. It is known that the solution pH can affect the surface charge of the adsorbent, the degree of ionization of the dyes, as well as the structure of the dye molecule [39,40]. Therefore, the solution pH is an important parameter during the dye adsorption processes. In order to study the surface charge of the adsorbent, the variation of the zeta potential at different pH values was investigated (Fig. 10). The surface charge of adsorbent assessed by point of zero charge (pH_{PZC}) is defined as the point where the zeta potential is zero. The surface charge is positive at pH value lower than pH_{PZC}, while it is negative at higher than pH_{PZC}. As shown in Fig. 10, the pH_{PZC} of the TMN sample was about 4.3.

According to the results and due to the cationic nature of the dyes (MB and VBB), in more acidic pH lower than 4.3, the repulsive forces between the cationic dyes and positive charges of the catalyst surface reduce the adsorption of dyes onto the catalyst and hence reduce the photocatalytic efficiency too. Also, a low pH is associated with a positively charged surface that cannot provide hydroxyl group, which are needed for hydroxyl radical formation. On the other hand, at pH values above the pH_{PZC}, the surface of the catalyst is negative, and hence, due to attractive forces between

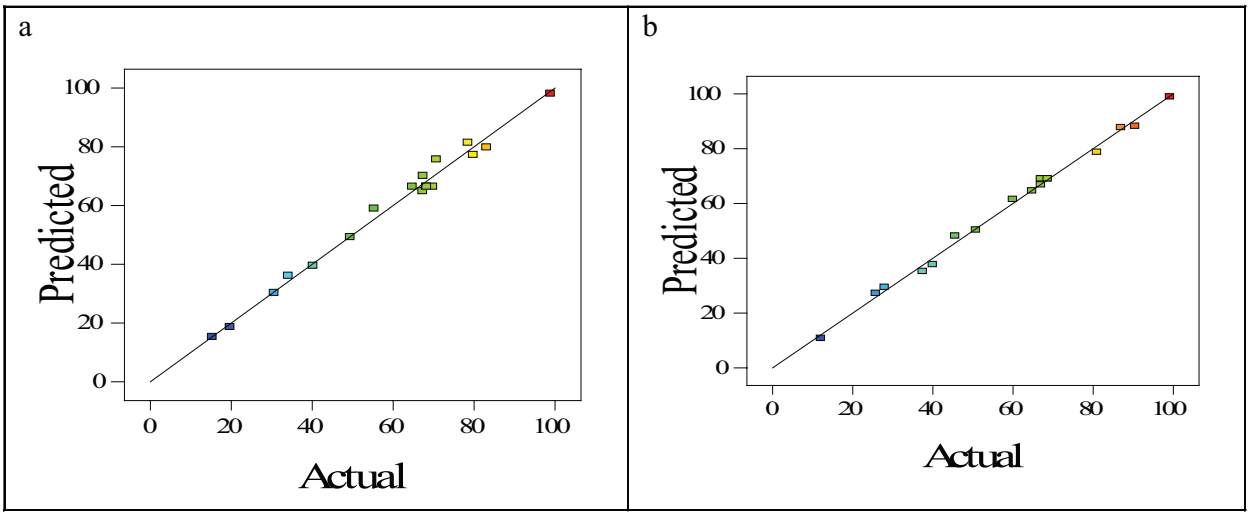

Fig. 8. Plot of predicted values of removal percentage vs. observed values for: (a) MB and (b) VBB.

Table 6
The coefficient estimates of quadratic model and significance of regression coefficients for MB

Terms	Coefficient estimate	MS[a]	*F*-value	*p*-value
Intercept	66.45	–	–	–
X_1	10.42	1085.76	95.01	<0.0001
X_2	5.42	293.76	25.71	0.0010
X_3	25.57	6539.27	572.25	<0.0001
X_1X_2	–0.88	6.12	0.53	0.4850
X_1X_3	0.95	7.22	0.63	0.4496
X_2X_3	3.72	111.01	9.71	0.0143
X_{12}	–6.74	123.08	10.77	0.0112
X_{22}	3.86	40.38	3.53	0.0969
X_{32}	–10.60	304.44	26.64	0.0009

[a]Mean squares.

Table 7
The coefficient estimates of reduced cubic model and significance of regression coefficients for VBB

Terms	Coefficient estimate	MS[a]	*F*-value	*p*-value
Intercept	68.99	–	–	–
X_1	25.25	1,275.13	261.22	<0.0001
X_2	21.75	946.12	193.82	<0.0001
X_3	18.69	3493.16	715.60	<0.0001
X_1X_2	3.91	122.46	25.09	0.0007
X_{12}	–6.05	113.41	23.23	0.0009
X_{22}	–12.05	450.01	92.19	<0.0001
$X_{12}X_2$	–8.51	115.94	23.75	0.0009
X_1X_{22}	–13.11	275.10	56.36	<0.0001

[a]Mean squares.

this negative surface and cationic MB and VBB molecules, more cationic dyes reach near the catalyst surface. As we expect, photocatalytic efficiency should be enhanced in more alkaline pH that favors hydroxyl radical producing [41].

To study the combined effect of pH values and catalyst dosage, the RSM was used, and the results were shown in Figs. 9(b) (left) and 9(a) (right). As can be seen in Fig. 9(b) (left), catalyst dosage had a significant effect on decolorization efficiency of MB; decolorization efficiency increased with increasing catalyst dosage at all applied pH value; and also, it increased with increasing pH. As catalyst dosage increases, total active surface area increases; therefore, more active sites on catalyst surface are accessible.

The surface plots of decolorization of MB and VBB are given in Fig. 9(c) (left) and (right), respectively. The decolorization increases with increase in catalyst dosage and irradiation time whereas pH kept constant at 6 being the central levels. This may be due to increases in the number of dye molecule adsorbed. Finally, based on the RSM results, the optimum values of the process variables for the maximum decolorization efficiency are X_1 = 1.6 g L^{-1}, X_2 = 9, and X_3 = 50 min for MB, and X_1 = 1.2 g L^{-1}, X_2 = 7.5, and X_3 = 105 min for VBB. After verifying by a further experimental test with the predicted values, the results indicated that the maximum decolorization efficiency was achieved when the values of each parameter were set as the optimum values, which was in good agreement with the predicted values.

3.5. Evaluation of catalyst stability

The feasibility of catalyst recovery and recycle in photocatalytic processes is most important, since it contributes significantly to lowering the cost of the photocatalytic decolorization of dyes. The reusability and stability of photocatalysts were investigated using 1.6 g L^{-1} of photocatalyst (Fig. 11). For each cycle, photocatalysts were reused for the decolorization of a fresh MB solution under similar conditions after the photocatalyst was separated by magnet, and then, it was washed with distilled water and dried at room temperature. As can be seen from Fig. 11, the catalytic activity of

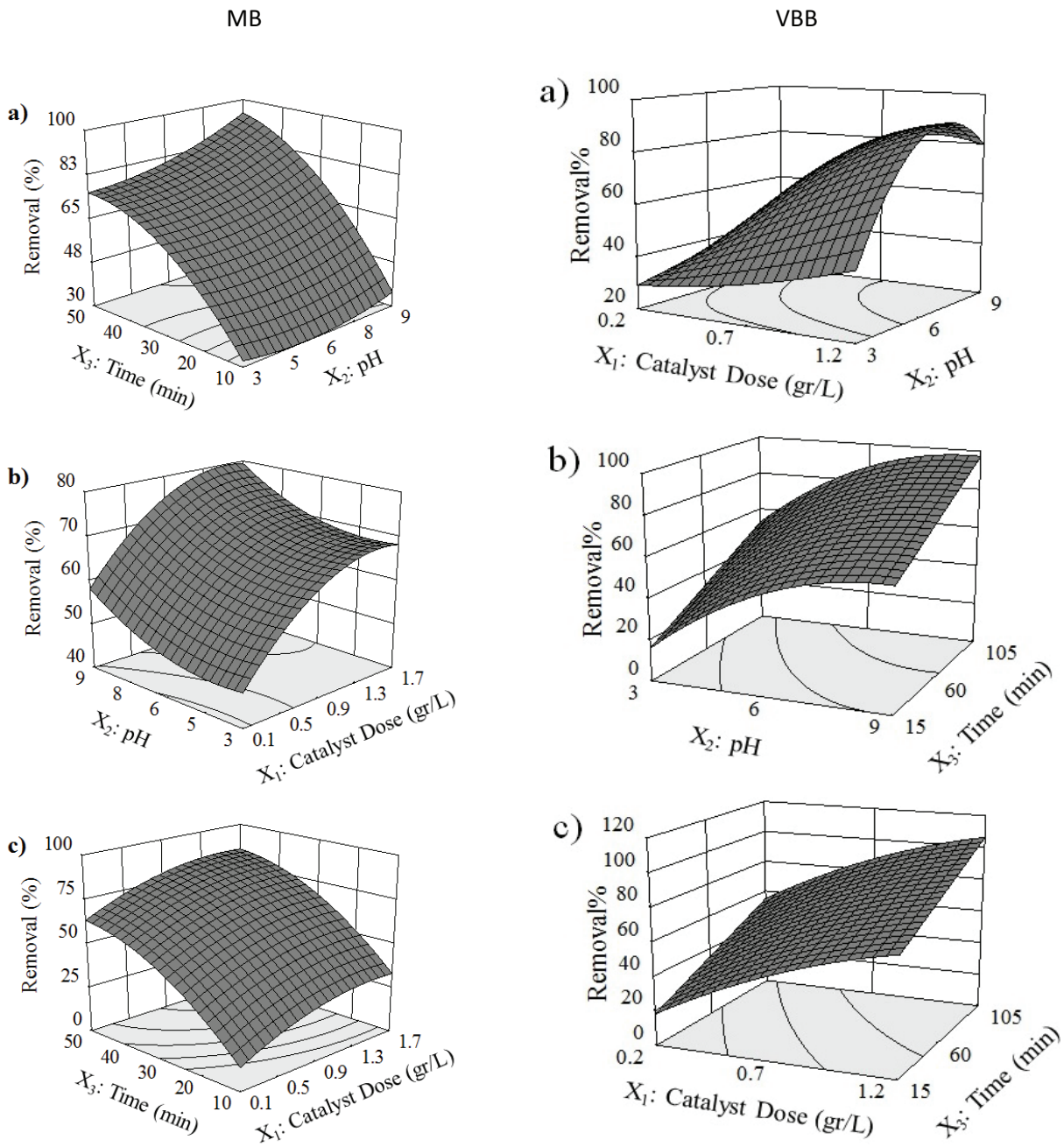

Fig. 9. Left: The response surface plots for removal of dye (%) as a function of time and pH (a), pH and catalyst dosage (b) and time and catalyst dosage (c) for MB. Right: The response surface plots for removal of dye (%) as a function of catalyst dosage and pH (a), pH and time (b), and catalyst dosage and time (c) for VBB.

the TiO_2 nanocomposite (TMN) did not significant change in four successive runs and the removal of MB remains about 90% and then decreased gradually. The decrease of decolorization efficiency may due to the adsorption of intermediate products on the photocatalyst active sites. However, 81% of MB was decolorized successfully for the fifth use of the photocatalysts, which indicated that theTiO_2 nanocomposite (TMN) catalyst was stable during the photodegradation of MB.

4. Conclusions

The new photocatalyst ($Fe_3O_4/SiO_2/TiO_2$ promoted with zinc composite or TMN) has been synthesized by a combination of sol–gel and wetness impregnation methods and characterized with SEM, XRD, BET, FTIR, and zeta potential sizer (ξ). Results of this research showed that hybridization of ZnO–TiO_2 semiconductors and supporting it on Fe_3O_4/SiO_2 nanoparticles can efficiently increase the photodegradation

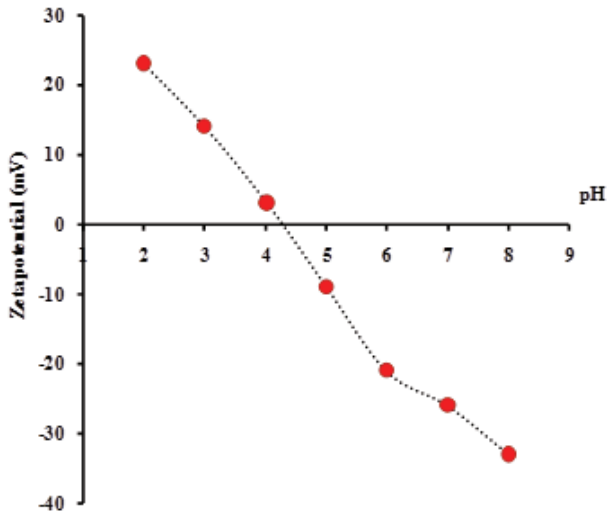

Fig. 10. Zeta potential titration as of pH of TMN dispersion.

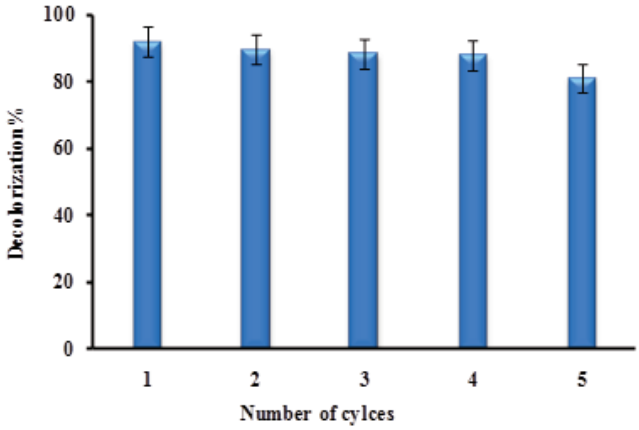

Fig. 11. Recycle and reuse of photocatalysts for MB decolorization (MB concentration: 30 mg L^{-1}, photocatalyst dosage: 1.6 g L^{-1}, pH: 9, irradiation time: 50 min).

activity of the obtained photocatalyst. Hence, the results confirm the effectiveness of the proposed TMN photocatalyst for the degradation of dyes from wastewater. Moreover, the magnetic TMN can be easily manipulated in magnetic field for desired separation, leading to the removal of dyes from polluted water. The decolorization efficiency of both the dyes MB and VBB using TMN in the presence of UV light was found to be comparatively higher than in the presence of visible light. Visible light will turn up as an alternative light source owing to its availability and nonhazardous nature; in spite of the fact that the UV irradiation can bring better results in the decolorization of dyes. A CCD was applied for multivariate optimization of the effects of three different parameters influencing the photocatalytic decolorization efficiency of the dye solution containing MB and VBB using UV/TMN nanocomposite process. RSM was used to investigate the individual effects and possible interactions between the most effective variables, including the reaction time, catalyst dosage, and pH solution. The effect of experimental parameters on the decolorization efficiency was illustrated by the response surface plot of the model-predicted responses. The results also indicated that pH plays an important role in the photodecolorization extent of the used dyes because of its effects on the charge of the catalyst surface. Predicted values were found to be in good agreement with experimental values (R^2 98.8% and 99.5% and adjusted R^2 = 98.0% and 99.1% for MB and VBB, respectively), which indicated suitability of the model and the success of CCD in optimization of decolorization process. Based on the RSM results, the optimum values of the process variables for the maximum decolorization efficiency are catalyst dosage = 1.6 g L^{-1}, pH = 9, and time = 50 min for MB, and catalyst dosage = 1.2 g L^{-1}, pH = 7.5, and time = 105 min for VBB. The photocatalytic stability of the TMN has also been checked. After six successive cycles, these TMNs were magnetically separated from the treated solution. The enhanced photocatalytic activity, excellent chemical stability, and fast magnetic separation make these multifunctional nanostructures potentially useful in practical settings of photocatalysis

Acknowledgment

The authors thank the research council of Razi University of Kermanshah (Iran) for the financial support.

References

[1] G. Zhang, F. Yang, M. Gao, X. Fang, L. Liu, Electro-Fenton degradation of azo dye using polypyrrole/anthraquinonedisulphonate composite film modified graphite cathode in acidic aqueous solutions, Electrochim. Acta, 53 (2008) 5155–5161.

[2] S. Qu, F. Huang, S. Yu, G. Chen, J. Kong, Magnetic removal of dyes from aqueous solution using multi-walled carbon nanotubes filled with Fe_2O_3 particles, J. Hazard. Mater., 160 (2008) 643–647.

[3] N. Daneshvar, M. Ayazloo, A.R. Khataee, M. Pourhassan, Biological decolorization of dye solution containing Malachite Green by microalgae *Cosmarium* sp., Bioresour. Technol., 98 (2007) 1176–1182.

[4] Y.M. Slokar, A.M. Le Marechal, Methods of decoloration of textile wastewaters, Dyes Pigm., 37 (1998) 335–356.

[5] C.A. Martinez-Huitle, E. Brillas, Decontamination of wastewaters containing synthetic organic dyes by electrochemical methods: a general review, Appl. Catal., B, 87 (2009) 105–145.

[6] A.R. Khataee, V. Vatanpour, A.R. Amani Ghadim, Decolorization of C.I. Acid Blue 9 solution by UV/Nano-TiO_2, Fenton, Fenton-like, electro-Fenton and electrocoagulation processes: a comparative study, J. Hazard. Mater., 161 (2009) 1225–1233.

[7] S. Mousavi-Mortazavi, A. Nezamzadeh-Ejhieh, Supported iron oxide onto an Iranian clinoptilolite as a heterogeneous catalyst for photodegradation of furfural in a wastewater sample, Desal. Wat. Treat., 57 (2016) 10802–10814.

[8] Z.-A. Mirian, A. Nezamzadeh-Ejhieh, Removal of phenol content of an industrial wastewater via a heterogeneous photodegradation process using supported FeO onto nanoparticles of Iranian clinoptilolite, Desal. Wat. Treat., 57 (2016) 16483–16494.

[9] A. Nezamzadeh-Ejhieh, Z. Banan, Photodegradation of dimethyldisulfide by heterogeneous catalysis using nano CdS and nano CdO embedded on the zeolite A synthesized from waste porcelain, Desal. Wat. Treat., 52 (2014) 16–18.

[10] A. Buthiyappan, A.R. Abdul Aziz, W.M.A. Wan Daud, Recent advances and prospects of catalytic advanced oxidation process in treating textile effluents, Rev. Chem. Eng., 32 (2016) 1–47.

[11] D.F. Laine, I.F. Cheng, The destruction of organic pollutants under mild reaction conditions: a review, Microchem. J., 85 (2007) 183–193.
[12] E. Brillas, I. Sirés, M.A. Oturan, Electro-Fenton process and related electrochemical technologies based on Fenton's reaction chemistry, Chem. Rev., 109 (2009) 6570–6631.
[13] D. Vione, C. Minero, V. Maurino, M.E. Carlotti, T. Picaionotto, E. Pelizzetti, Degradation of phenol and benzoic acid in the presence of a TiO_2 based heterogeneous photocatalyst, Appl. Catal., B, 58 (2005) 79–88.
[14] K. Rajeshwar, M.E. Osugi, W. Chanmanee, C.R. Chenthamarakshan, M.V.B. Zanoni, P. Kajitvichyanukul, R. Krishnan-Ayer, Heterogeneous photocatalytic treatment of organic dyes in air and aqueous media, J. Photochem. Photobiol., C, 9 (2008) 171–192.
[15] T. Nikolaos, V. Belessi, D. Lambropoulou, Photocatalytic degradation of Reactive Red using anatase/brookite TiO_2 mesoporous nanoparticles: optimization using response surface methodology (RSM) and kinetics studies, Environ. Sci. Pollut. Res., 20 (2013) 2305–2320.
[16] T. Harifi, M. Montazer, A novel magnetic reusable nanocomposite with enhanced, photocatalytic activities for dye degradation, Sep. Purif. Technol., 134 (2014) 210–219.
[17] R. Li, Y. Jia, N. Bu, J. Wu, Q. Zhen, Photocatalytic degradation of methyl blue using Fe_2O_3/TiO_2 composite ceramics, J. Alloys Compd., 643 (2015) 88–93.
[18] Z.-D. Li, H.-L. Wang, X.-N. Wei, X.-Y. Liu, Y.-F. Yang, W.-F. Jiang, Preparation and photocatalytic performance of magnetic Fe_3O_4@ TiO_2 core-shell microspheres supported by silica aerogels from industrial fly ash, J. Alloys Compd., 659 (2016) 240–247.
[19] H. Zabihi-Mobarakeh, A. Nezamzadeh-Ejhieh, Application of supported TiO_2 onto Iranian clinoptilolite nanoparticles in the photodegradation of mixture of aniline and 2,4-dinitroaniline aqueous solution, J. Ind. Eng. Chem., 26 (2014) 315–321.
[20] A. Nezamzadeh-Ejhieh, M. Bahrami, Investigation of the photocatalytic activity of supported ZnO–TiO_2 on clinoptilolite nano-particles towards photodegradation of wastewater-contained phenol, Desal. Wat. Treat., 55 (2015) 1096–1104.
[21] R. Abazari, A.R. Mahjoub, S. Sanati, Magnetically recoverable Fe_3O_4-ZnO/AOT nanocomposites: synthesis of a core–shell structure via a novel and mild route for photocatalytic degradation of toxic dyes, J. Mol. Liq., 223 (2016) 1133–1142.
[22] R. Saravanan, M.M. Khan, V.K. Gupta, E. Mosquera, F. Gracia, V. Narayanang, A. Stephen, ZnO/Ag/Mn_2O_3 nanocomposite for visible light-induced industrial textile effluent degradation, uric acid and ascorbic acid sensing and antimicrobial activity, RSC Adv., 5 (2015) 34645–34651.
[23] S. Chaudhary, Y. Kaur, A. Umar, G.R. Chaudhary, 1-butyl-3-methylimidazolium tetrafluoroborate functionalized ZnO nanoparticles for removal of toxic organic dyes, J. Mol. Liq., 220 (2016) 1013–1021.
[24] J. Esmaili-Hafshejani, A. Nezamzadeh-Ejhieh, Increased photocatalytic activity of Zn(II)/Cu(II) oxides and sulfides by coupling and supporting them onto clinoptilolite nanoparticles in the degradation of benzophenone aqueous solution, J. Hazard. Mater., 316 (2016) 194–203.
[22] M. Sadeghi, Z. Nematifar, M. Irandoust, N. Fattahi, P. Hamzei, A. Barati, M. Ramezani, M. Shamsipur, Efficient and selective extraction and determination of ultra trace amounts of Hg^{2+} using solid phase extraction combined with ion pair based surfactant-assisted dispersive liquid–liquid microextraction, RSC Adv., 5 (2015) 100511–100521.
[23] M. Nosuhi, A. Nezamzadeh-Ejhieh, High catalytic activity of Fe(II)-clinoptilolite nanoparticles for indirect voltammetric determination of dichromate: experimental design by response surface methodology (RSM), Electrochim. Acta, 223 (2017) 47–62.
[24] M. Sadeghi, M. Irandoust, F. Khorshidi, M. Feyzi, F. Jafari, T. Shojaeimehr, M. Shamsipur, Removal of Arsenic(III) from natural contaminated water using magnetic nanocomposite: kinetics and isotherm studies, J. Iran. Chem. Soc., 13 (2016) 1175–1188.
[25] M. Feyzi, E. Shahbazi, Catalytic performance and characterization of Cs–Ca/SiO_2–TiO_2 nanocatalysts for biodiesel production, J. Mol. Catal. A: Chem., 404 (2015) 131–138.
[26] L. Vafayi, S. Gharibe, Enhancement of photocatalytic activity of ZnO–SiO_2 by nano-sized Pt for efficient removal of dyes from wastewater effluents, Iran. J. Catal., 5 (2015) 365–371.
[27] F. Gözüak, Y. Köseoğlu, A. Baykal, H. Kavas, Synthesis and characterization of $CoxZn1-xFe_2O_4$ magnetic nanoparticles via a PEG-assisted route, J. Magn. Magn. Mater., 321 (2009) 2170–2177.
[28] K.Y. Jung, S.B. Park, Enhanced photoactivity of silica-embedded titania particles prepared by sol–gel process for the decomposition of trichloroethylene, Appl. Catal., B, 25 (2000) 249–256.
[29] X. Gao, I.E. Wachs, Titania–silica as catalysts: molecular structural characteristics and physico-chemical properties, Catal. Today, 51 (1999) 233–254.
[30] M.M. Mohamed, T.M. Salama, T. Yamaguchi, Synthesis, characterization and catalytic properties of titania–silica catalysts, Colloids Surf., A, 207 (2002) 25–32.
[31] C.L. Luu, Q.T. Nguyen, S.T. Ho, Synthesis and characterization of Fe-doped TiO_2 photocatalyst by the sol–gel method, Adv. Nat. Sci. Nanosci. Nanotechnol., 1 (2010) 5–10.
[32] A. Nezamzadeh-Ejhieh, A. Shirzadi, Enhancement of the photocatalytic activity of Ferrous Oxide by doping onto the nano-clinoptilolite particles towards photodegradation of tetracycline, Chemosphere, 107 (2014) 136–144.
[33] D. Predoi, O. Crisan, A. Jitianu, M.C. Valsangiacom, M. Raileanu, M. Crisan, M. Zaharescu, Iron oxide in a silica matrix prepared by the sol–gel method, Thin Solid Films, 515 (2007) 6319–6323.
[34] A. Nezamzadeh-Ejhieh, S. Hushmandrad, Solar photodecolorization of methylene blue by CuO/X zeolite as a heterogeneous catalyst, Appl. Catal., A, 388 (2010) 149–159.
[35] A. Nezamzadeh-Ejhieh, M. Karimi-Shamsabadi, Comparison of photocatalytic efficiency of supported CuO onto micro and nano particles of zeolite X in photodecolorization of Methylene blue and Methyl orange aqueous mixture, Appl. Catal., A, 477 (2014) 83–92.
[36] G.K. Parshetti, A.A. Telke, D.C. Kalyani, S.P. Govindwar, Decolorization and detoxification of sulfonated azo dye methyl orange by Kocuria rosea MTCC 1532, J. Hazard. Mater., 176 (2010) 503–509.
[37] H. Derikvandi, A. Nezamzadeh-Ejhieh, Comprehensive study on enhanced photocatalytic activity of heterojunction ZnS-NiS/zeolite nanoparticles: experimental design based on response surface methodology (RSM), impedance spectroscopy and GC-MASS studies, J. Colloid Interface Sci., 490 (2017) 652–664.
[38] H. Derikvandi, A. Nezamzadeh-Ejhieh, Designing of experiments for evaluating the interactions of influencing factors on the photocatalytic activity of NiS and SnS_2: focus on coupling, supporting and nanoparticles, J. Colloid Interface Sci., 490 (2017) 628–641.
[39] A. Nezamzadeh-Ejhieh, M. Karimi-Shamsabadi, Decolorization of a binary azo dyes mixture using CuO incorporated nanozeolite-X as a heterogeneous catalyst and solar irradiation, Chem. Eng. J., 228 (2013) 631–641.
[40] A. Nezamzadeh-Ejhieh, H. Zabihi-Mobarakeh, Heterogeneous photodecolorization of mixture of methylene blue and bromophenol blue using CuO-nano-clinoptilolite, J. Ind. Eng. Chem., 20 (2014) 1421–1431.
[41] F. Chen, Y. Xie, J. Zhao, G. Lu, Photocatalytic degradation of dyes on a magnetically separated photocatalyst under visible and UV irradiation, Chemosphere, 44 (2000) 1159–1168.